The cerium magnetic form factor and diffuse polarization in $CeRh_3B_2$ as functions of temperature

2004 J. Phys.: Condens. Matter 16 1211

(http://iopscience.iop.org/0953-8984/16/8/007)

INSTITUTE OF PHYSICS PUBLISHING JOURNAL OF PHYSICS: CONDENSED MATTER

J. Phys.: Condens. Matter **16** (2004) 1211–1230 PII: S0953-8984(04)72252-3

The cerium magnetic form factor and diffuse polarization in $CeRh_3B_2$ as functions of temperature

F Givord[1,4,5], **J-X Boucherle**[1,5], **E Lelièvre-Berna**[2] **and P Lejay**[3]

[1] CEA-Grenoble, DSM/DRFMC/SPSMS/MDN, 38054 Grenoble Cedex 9, France
[2] Institut Laue-Langevin, BP156, 38042 Grenoble Cedex 9, France
[3] CRTBT, CNRS, 166X, 38042 Grenoble Cedex 9, France

E-mail: givord@drfmc.ceng.cea.fr

Received 19 November 2003
Published 13 February 2004
Online at stacks.iop.org/JPhysCM/16/1211 (DOI: 10.1088/0953-8984/16/8/007)

Abstract

In the compound $CeRh_3B_2$, a rather special polarization of the conduction electrons along the ***c***-chains of cerium atoms had been previously reported at low temperatures (Alonso *et al* 1998 *J. Magn. Magn. Mater.* **177–181** 1048). The distribution of the $CeRh_3B_2$ magnetization has now been studied as a function of temperature up to 150 K—that is, above the Curie temperature of 115 K. The magnetization density maps have been obtained from polarized neutron diffraction experiments by using the maximum entropy method. The cerium form factor has also been analysed. Calculations of the form factor including several multiplets are developed and it is shown that it is necessary to take into account the influence of the higher multiplet of the Ce^{3+} ion. This result is coherent with the observation of a peak at high energy in the inelastic neutron spectra, indicating a very large crystal electric field splitting. Both analyses lead to the same conclusion that, on heating, the diffuse negative magnetization observed at low temperature along the cerium chains disappears at the magnetic ordering temperature. The influence of the second multiplet of the Ce^{3+} ion could be part of the explanation for the low value of the 4f moment and the large Curie temperature in $CeRh_3B_2$.

1. Introduction

The ternary cerium boride $CeRh_3B_2$ shows ferromagnetic ordering with an unusually high Curie temperature, $T_c = 115$ K [1]. It is by far the highest magnetic ordering temperature of any cerium compound with non-magnetic elements. The isostructural compound $GdRh_3B_2$ has a Curie temperature of 93 K and a simple de Gennes scaling would lead to a Curie temperature

[4] Author to whom any correspondence should be addressed.
[5] CNRS staff.

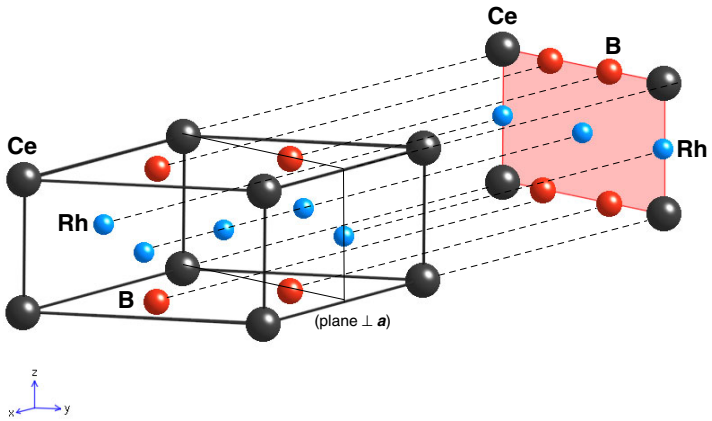

Figure 1. The crystallographic structure of $CeRh_3B_2$ and its projection on a plane perpendicular to the a-direction of the hexagonal structure.

(This figure is in colour only in the electronic version)

value of ≈1 K for $CeRh_3B_2$—that is, two orders of magnitude lower than the real value. Its magnetic properties are highly anisotropic. The easy magnetization is within the c-plane and the saturation magnetization is only 0.4 μ_B/formula unit, a value which is strongly reduced compared to the cerium free ion value (2.14 μ_B). The magnetization along the hard c-axis is about five times less than that along the easy direction. From measurements performed in the paramagnetic state up to 800 K [2, 3], it is found that the magnetic susceptibility follows a Curie–Weiss law only above 600 K.

$CeRh_3B_2$ crystallizes in the hexagonal $CeCo_3B_2$-type structure (figure 1). Rhodium atoms lie in planes at $z = 1/2$, whereas the boron and the cerium atoms are in the basal plane. There is only one site of cerium atoms, located at the origin of the cell (point symmetry $6/mmm$). Along the c-axis, they form chains with very short Ce–Ce distances (3.04 Å), much shorter than in the c-plane (5.48 Å). This feature was invoked as lying the origin of the anomalous magnetic properties, especially those leading to hybridization between cerium 4f and conduction electrons and to strong crystal electric field effects [4, 5]. This last property has been confirmed by inelastic neutron spectroscopy measurements performed with high incident energy at ISIS (UK). The observed transition corresponds to a crystal field splitting of the order of 2000 K [6], a value which is not negligible when compared to the difference between the cerium ground multiplet $J = 5/2$ and the excited multiplet $J' = 7/2$ lying at around 3250 K [7]. Contributions from the excited multiplet can then be present in the wavefunctions of all energy levels, even the fundamental one.

A polarized neutron diffraction study [8], performed at $T = 7$ K in the ferromagnetic state indicated localization of the magnetization density and confirmed the anisotropic character of the magnetic properties. The magnetization at low temperature is distributed as follows:

(i) no magnetization on the rhodium and boron sites;
(ii) a 4f-type moment, with a definite asymmetry, localized on the cerium site; and
(iii) a large negative diffuse contribution of 5d type, very anisotropic, lying between the cerium atoms along the c-chains only.

Because of this negative diffuse contribution, the value of the 4f moment is quite different from the value of the measured magnetization. It is therefore important to know the thermal

Table 1. Parameters of the crystal structure of $CeRh_3B_2$ at low temperature. The b are the Fermi lengths and the B the Debye–Waller factors. The absorption coefficient at this wavelength is $\mu = 4.0\ cm^{-1}$. Space group: $P6/mmm$; $a = 5.456$ Å, $c = 3.037$ Å.

Site	x	y	z	b (fm)	B (Å^2)
Ce (1a)	0	0	0	4.84	0.18
Rh (3g)	1/2	0	1/2	5.88	0.12
B (2c)	1/3	2/3	0	6.56	0.18

dependence of this diffuse contribution to deduce the thermal variation of the 4f moment. Polarized neutron diffraction measurements similar to those at 7 K [8] were undertaken at various temperatures up to 150 K. Magnetization density maps were obtained and the cerium 4f form factor was calculated. Because of the very large crystal field splitting, the calculation takes into account the presence of the two cerium multiplets.

2. Experimental details and results

The experiments at different temperatures were performed on the D3 diffractometer at the ILL (Grenoble, France), at a wavelength $\lambda = 0.852$ Å. The magnetic field was applied parallel to the easy magnetization direction $\boldsymbol{a}$. Its value was 5 T, except at $T = 150$ K where it was increased to 9 T in order to induce a larger moment and get a better precision. The former experiment ($T = 7$ K and $H = 4.6$ T) was performed at the LLB (Saclay, France).

The crystal studied, $CeRh_3B_2$, was the same as that already measured in [8]. It was produced using 99% enriched ^{11}B to avoid the large neutron absorption cross section due to ^{10}B. Its shape is a platelet of $2.0 \times 1.5 \times 3.6\ mm^3$, the first dimension being along the $\boldsymbol{a}$-direction and the last one along the $\boldsymbol{c}$-direction. Its characteristics had already been determined for the previous study. The values used for the treatment of our data are given in table 1. The extinction factor g, deduced from polarized neutron diffraction experiments at several wavelengths [8], is 700(100) rad^{-1}.

Measurements of the flipping ratios $R = I^+/I^- = (1+\gamma)^2/(1-\gamma)^2$ of the Bragg reflections hkl yield values of $F_M(hkl)$ through $\gamma = F_M/F_N$, where F_N and F_M are the nuclear and magnetic structure factors, respectively. The flipping ratios of 30 independent reflections of type $0kl$ were measured at four temperatures: 7 K for a rapid check of the previous results [8], 110 and 120 K around the ordering temperature, and 150 K above the ordering temperature. The first six reflections at low diffraction angle were also measured at various intermediate temperatures. In order to take into account the imperfections of the instrument, appropriate corrections (polarization of the incident beam, flipping efficiency, $\lambda/2$ corrections) were applied and the nuclear structure factors F_N were calculated using the parameters of table 1.

3. Magnetization density maps

The $F_M(hkl)$ are the Fourier components of the magnetization density $M(\boldsymbol{r})$. The projection of this density on a plane perpendicular to the $\boldsymbol{a}$-direction was calculated using the 2D maximum entropy method (MaxEnt) [9]. This method yields the most probable magnetization distribution map compatible with the measured $F_M(hkl)$, taking into account their error bars. Its main advantage, compared to the classical Fourier inversion, is that it makes no assumption concerning the unmeasured Fourier components and avoids the oscillations due to truncation effects. The number of pixels was chosen as 32×62 respectively along the [001]

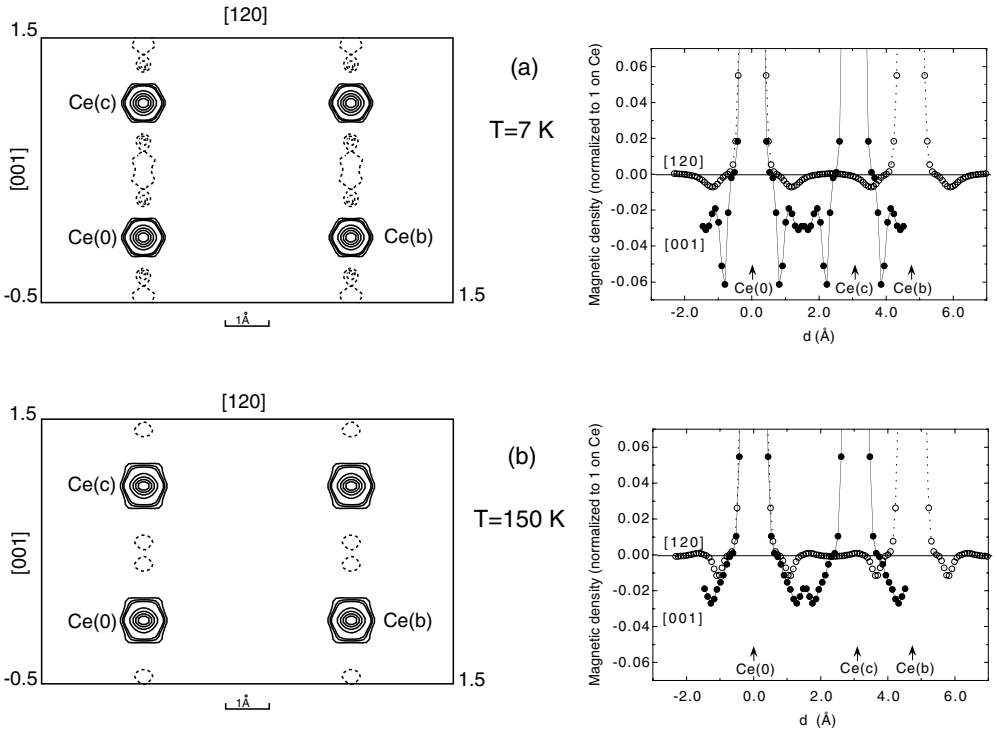

Figure 2. Left-hand side: projections along the a-direction of the magnetization distribution obtained with MaxEnt in $CeRh_3B_2$. Full/dashed lines correspond to positive/negative contours. (a) $T = 7$ K, the separation between the contour lines is 0.045 μ_B Å^{-2} for the negative and the three first positive low contours and 0.450 μ_B Å^{-2} around the cerium sites. (b) $T = 150$ K, the separation between the contour lines is 0.008 μ_B Å^{-2} for the negative and the three first positive low contours and 0.076 μ_B Å^{-2} around the cerium sites. Right-hand side: the projected magnetic density drawn between two cerium atoms along the [001] and [120] directions. The values are normalized to the maximum value on the cerium atoms, that is 2.73 μ_B Å^{-2} at $T = 7$ K (a) and 0.417 μ_B Å^{-2} at $T = 150$ K (b).

and [120] directions of the direct space (the [001] and [010] directions of reciprocal space). The projected maps have thus been obtained at the four temperatures 7, 110, 120 and 150 K. The $F_M(000)$ value is the bulk magnetization measured in the same experimental conditions—that is, for 0.42(1), 0.25(1), 0.17(1) and 0.087(5) μ_B, respectively. The field dependence of the magnetization measured in the paramagnetic state at 150 K up to 10 T is perfectly linear.

The maps obtained for the lowest ($T = 7$ K [8]) and the highest ($T = 150$ K) temperatures are shown in the left-hand side of figure 2. The corresponding projection of the atoms can be seen in figure 1. At 7 K, in the ferromagnetic state (figure 2(a)), the results are those already mentioned in the previous study:

(i) no magnetization is found on the rhodium atoms which are located on one unique site (see the rhodium projected in (1/2, 1/2));
(ii) a 4f-type density is localized on the cerium site; and
(iii) a large negative diffuse contribution is observed between the cerium atoms along the c-chains only.

At 150 K, in the paramagnetic state, this negative diffuse density has almost disappeared (figure 2(b)). The density between the cerium atoms is more detailed on the right-hand side

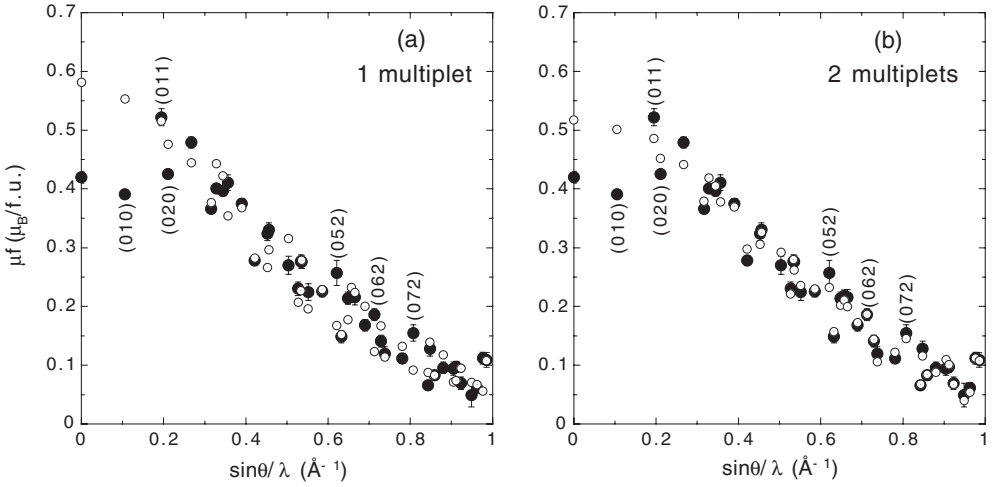

Figure 3. Comparison of the experimental (full dots) with the calculated (open dots) magnetic amplitudes μf at $T = 7$ K. (a) Calculation with one multiplet $J = 5/2$; (b) calculation with two multiplets $J = 5/2$ and $J' = 7/2$. Calculations were performed using the wavefunction coefficients.

Table 2. Refined wavefunction coefficients $a_{J,M}$ from data at $T = 7$ K. N_J is the number of multiplets, K_0 a scaling factor of the moment, μ_{4f} the calculated 4f moment and μ_{4f}^S its spin part.

N_J	$a_{\frac{7}{2},\frac{7}{2}}$	$a_{\frac{5}{2},\frac{5}{2}}$	$a_{\frac{5}{2},\frac{3}{2}}$	$a_{\frac{5}{2},\frac{1}{2}}$	$a_{\frac{5}{2},\frac{-1}{2}}$	$a_{\frac{5}{2},\frac{-3}{2}}$	$a_{\frac{5}{2},\frac{-5}{2}}$					
	$a_{\frac{7}{2},\frac{5}{2}}$	$a_{\frac{7}{2},\frac{3}{2}}$	$a_{\frac{7}{2},\frac{1}{2}}$	$a_{\frac{7}{2},\frac{-1}{2}}$	$a_{\frac{7}{2},\frac{-3}{2}}$	$a_{\frac{7}{2},\frac{-5}{2}}$	$a_{\frac{7}{2},\frac{-7}{2}}$	K_0	μ_{4f} (μ_B)	μ_{4f}^S (μ_B)	χ^2
1	0	0.323	0	−0.687 (44)	0	0.650 (47)					
	0	0	0	0	0	0	0	0.6 (1)	0.58	−0.2	9.4
2	0	0.207 (100)	0	0.570 (40)	0	0.656 (48)					
	0.290 (30)	0	0.154 (102)	0	−0.197	0	0.235 (51)	0	0.66	0.52	−0.3	1.9

of figure 2 where these densities along the [001] or [120] directions are drawn for the two temperatures. It is quite clear that at $T = 7$ K the densities along the two directions are very different: it is strongly negative along [001] whereas it is around zero along [120]. At $T = 150$ K, the density along [001] has strongly decreased whereas the density along [120] is unchanged.

4. Form factor

The $F_M(hkl)$ can be directly analysed in reciprocal space (see figures 3 and 4, plain dots). They correspond to the sums of two magnetic amplitudes $\mu f(\boldsymbol{Q})$ centred on the cerium site, where μ is the magnetic moment and $f(\boldsymbol{Q})$ the associated magnetic form factor for the scattering vector $\boldsymbol{Q}$ ($|\boldsymbol{Q}| = 4\pi \sin\theta/\lambda$). One magnetic amplitude is of 4f type and is observed up to $\sin\theta/\lambda = 1.0$ Å^{-1}. The negative and anisotropic second one, of 5d type, is very delocalized

and vanishes at $\sin\theta/\lambda \approx 0.2$ Å^{-1}. Reflections lying above this value are then characteristic of the 4f contribution only. Therefore, the first three reflections 010, 011 and 020, as well as 000 given by the macroscopic magnetization, were not used for the refinements of the 4f contribution.

4.1. Calculation using the ground state wavefunction

The 4f cerium magnetic form factor can be calculated (appendix A) from the coefficients a_{JM} of the ground state wavefunction:

$$|\psi\rangle = \sum_{JM} a_{JM}|\theta JM\rangle, \qquad \text{with } \sum_{JM} a_{JM}^2 = 1.$$

The number of coefficients a_{JM} depends on the J multiplet considered, and, as mentioned in the introduction, the influence of the excited multiplet may be significant. There are six values associated with the ground multiplet $J = 5/2$ ($-5/2 \leqslant M \leqslant 5/2$) and eight values associated with the excited multiplet $J' = 7/2$ ($-7/2 \leqslant M' \leqslant 7/2$). As the magnetic field is applied along the $\boldsymbol{a}$-direction, this direction was taken as the quantification axis z for all the calculations (the $\boldsymbol{c}$-direction of the hexagonal structure is then the y-axis). z being a twofold axis implies that only terms corresponding to $\Delta M = \pm 2$ will exist [10]. Half of the coefficients a_{JM} are then zero:

$$a_{\frac{5}{2},\frac{5}{2}} = a_{\frac{5}{2},\frac{1}{2}} = a_{\frac{5}{2},\bar{\frac{3}{2}}} = 0,$$
$$a_{\frac{7}{2},\frac{5}{2}} = a_{\frac{7}{2},\frac{1}{2}} = a_{\frac{7}{2},\bar{\frac{3}{2}}} = a_{\frac{7}{2},\bar{\frac{7}{2}}} = 0.$$

For low temperatures ($T = 7$ K), when only the ground state is occupied, we have written a program which refines the coefficients a_{JM} of its wavefunction. A scaling factor K_0 is introduced, which can represent a reduction factor of the moment due to the strong hybridization effects [11]. This type of refinement leads to a wavefunction fitting the experimental data and does not need any model describing the state of the system.

A first refinement was tried by considering the ground multiplet $J = 5/2$ only. There remain only the three $a_{5/2,M}$ coefficients. The best fit corresponds to χ^2 around 9 ($\chi^2 = \sum_i p_i(\mu f_i^{\text{obs}} - \mu f_i^{\text{calc}})^2/(N_{\text{obs}} - N_{\text{var}})$ with $p_i = 1/\sigma_i^2$), with $a_{5/2,3/2}$ and $a_{5/2,-5/2}$ positive and $a_{5/2,-1/2}$ strongly negative (see table 2). The calculated points are plotted in figure 3(a). Besides the discrepancy for the reflections at low $\sin\theta/\lambda$ in which the 5d contribution is present and which were not used for the refinement anyway, the measured anisotropy is not at all well accounted for. In particular, the reflections of type $0k2$ are calculated to be much lower than those measured.

The fit is substantially improved if the two multiplets $J = 5/2$ and $J' = 7/2$ are taken into account (seven coefficients $a_{J,M}$) and is not much altered by the value of K_0 ($1.6 < \chi^2 < 1.9$). The results in table 2 are given for a value $K_0 = 0.66$, for coherence with what follows in this paper. The main change from the preceding calculation is the change of sign of the coefficient $a_{5/2,-1/2}$ and the emergence of non-negligible terms $a_{7/2,M'}$. The calculated 4f moment μ_{4f} ($0.52\ \mu_B$) is lower than that obtained with one multiplet ($0.58\ \mu_B$) but still definitely larger than the measured macroscopic magnetization $M = 0.42\ \mu_B$. The agreement between observed and calculated points (figure 3(b)) is much better for all the reflections and the calculation for $0k2$-type reflections is now quite satisfactory.

4.2. Calculation using the Hamiltonian

Another way of performing the calculations consists of a diagonalization of the Hamiltonian of the system to obtain the wavefunction coefficients of all the energy states. The form factor

Table 3. Examples of possible crystal field parameters $(B_k^q)_c$ fitting the Ce form factor. $J_{ff} = 570$ K, $(B_2^0)_c = -7500$ K, $(B_4^0)_c = 650$ K and $(B_6^6)_c = 0$. K_0 a scaling factor, μ_{4f} the calculated 4f moment, μ_{4f}^S its spin part and M the measured magnetization.

T (K)	H (T)	$(B_6^0)_c$ (K)	K_0	μ_{4f} (μ_B)	μ_{4f}^S (μ_B)	M (μ_B)	$M - \mu_{4f}$ (μ_B)	χ^2
7	4.6	−337(14)	0.66(2)	0.50	−0.52	0.42(1)	−0.08(1)	2.0
110	5	−331(30)	0.68(1)	0.26	−0.26	0.25(1)	−0.01(1)	2.4
120	5	−332(45)	0.68(9)	0.17	−0.18	0.17(1)	0.00(1)	1.7
150	9	−314(34)	0.68(4)	0.082	−0.071	0.087(5)	0.005(5)	1.3

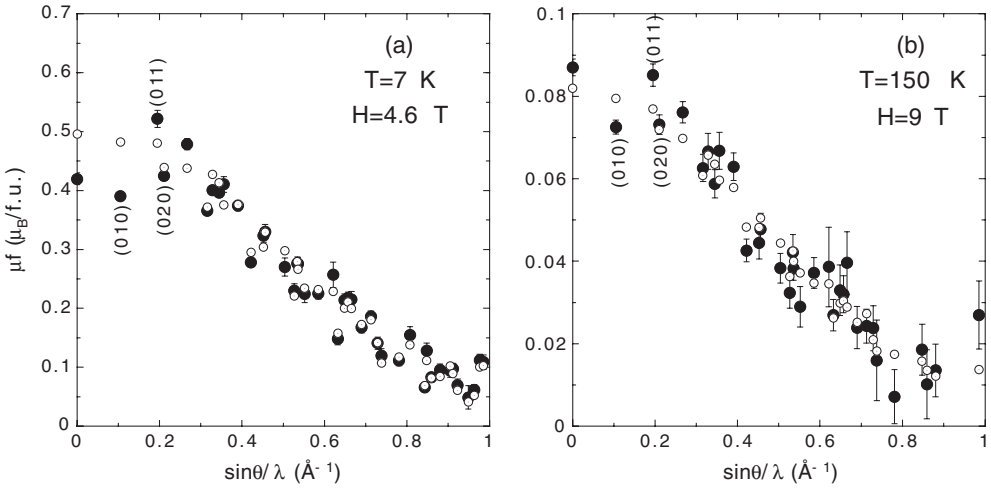

Figure 4. Comparison of the experimental magnetic amplitudes μf (full dots) with those calculated with two multiplets $J = 5/2$ and $J' = 7/2$ (open dots). (a) At $T = 7$ K; (b) at $T = 150$ K. Calculations were performed using exchange and crystal field parameters given in table 3.

is then calculated for each level and the resulting value is obtained taking into account the level populations. Such a calculation is necessary for data at high temperatures, when several levels might be occupied.

The Hamiltonian depends on exchange and crystal field parameters as defined in appendix B and we have written a program that can refine these parameters from the form factor data. At the same time, the spin and orbital parts of the moment are calculated. In fact, all these parameters are strongly correlated and some of them have been fixed. The value of the exchange parameter J_{ff} was estimated from calculations of the thermal variation of the magnetization and comparison to the Curie temperature. Calculations with two multiplets and a value of $J_{ff} = 570$ K lead to a Curie temperature around 115 K.

There are nine crystal field parameters B_k^q involved in the crystal field Hamiltonian for the twofold axis $\boldsymbol{a}$ as the quantification axis ($(B_2^0)_a$, $(B_2^2)_a$, $(B_4^0)_a$, $(B_4^2)_a$, $(B_4^4)_a$, $(B_6^0)_a$, $(B_6^2)_a$, $(B_6^4)_a$ and $(B_6^6)_a$). However, there are only four coefficients ($(B_2^0)_c$, $(B_4^0)_c$, $(B_6^0)_c$ and $(B_6^6)_c$) if the quantification axis is the sixfold axis $\boldsymbol{c}$. The nine coefficients for $\boldsymbol{z} = \boldsymbol{a}$ are not independent but are related to the four coefficients for $\boldsymbol{z} = \boldsymbol{c}$, using the matrix for rotation of spherical harmonics Y_k^q (Wigner formula). The relations are the following:

$$
\begin{aligned}
(B_2^0)_a &= -(1/2)(B_2^0)_c,\\
(B_2^2)_a &= -(3/2)(B_2^0)_c,\\
(B_4^0)_a &= (3/8)(B_4^0)_c,\\
(B_4^2)_a &= (5/2)(B_4^0)_c,\\
(B_4^4)_a &= (35/8)(B_4^0)_c,\\
(B_6^0)_a &= (1/16)(-5(B_6^0)_c + (B_6^6)_c),\\
(B_6^2)_a &= (1/32)(-105(B_6^0)_c - 15(B_6^6)_c),\\
(B_6^4)_a &= (1/16)(-63(B_6^0)_c + 3(B_6^6)_c),\\
(B_6^6)_a &= (1/32)(-231(B_6^0)_c - (B_6^6)_c).
\end{aligned}
$$

For simplicity, we use the four coefficients $(B_2^0)_c$, $(B_4^0)_c$, $(B_6^0)_c$ and $(B_6^6)_c$ for $\boldsymbol{z} = \boldsymbol{c}$, and the program calculates the corresponding nine coefficients for $\boldsymbol{z} = \boldsymbol{a}$. A possible reduction factor of the moment K_0 is also introduced.

As for the previous calculations, refinements of the data at $T = 7$ K have been tried first, by considering the ground multiplet $J = 5/2$ only ($(B_6^0)_c = (B_6^6)_c = 0$). No better result than $\chi^2 \simeq 15$ could be found. Calculations with the two multiplets were then undertaken. The spin–orbit coupling coefficient λ was fixed to 930 K ($\lambda = \Delta/J'$ with $\Delta = 3250$ K [7]). We have noticed that there are an infinity of sets of $(B_k^q)_c$ parameters which correspond to a wavefunction close to that given in table 2, and then to good reliability factors $\chi^2 \simeq 2$. Data collected at low temperature (7 K) and at higher temperatures (110, 120 and 150 K) were used to reduce the number of $(B_k^q)_c$ parameter sets. $(B_2^0)_c$ has to be negative to get the moment along the $\boldsymbol{a}$-direction. Various values of $(B_2^0)_c$ were tried as well as compatible values for $(B_4^0)_c$. $(B_6^6)_c$ has almost no influence on the form factor and was therefore fixed to zero. Only $(B_6^0)_c$ and K_0 were refined. No solution could be found with $K_0 = 1$ and its value is always found between 0.6 and 0.7. As an example, figure 4 shows the results obtained at $T = 7$ and 150 K for $(B_2^0)_c = -7500$ K, $(B_4^0)_c = 650$ K and $J_{\mathrm{ff}} = 570$ K. Table 3 gives the refined parameters $(B_6^0)_c$ and K_0 at the four temperatures, together with the corresponding calculated 4f moment $\mu_{4\mathrm{f}}$. These parameters are refined to almost the same values within the error bars and one can then consider that the set of values $(B_2^0)_c = -7500$ K, $(B_4^0)_c = 650$ K, $(B_6^0)_c = -350$ K, $(B_6^6)_c = 0$, $J_{\mathrm{ff}} = 570$ K and $K_0 = 0.67$ fit our results well. As mentioned above, other solutions for other values of $(B_2^0)_c$ lead after refinement to the same values of χ^2 and $\mu_{4\mathrm{f}}$. The determination of the right set of parameters needs data of another type: the treatment of the inelastic neutron spectroscopy data together with the magnetization and susceptibility thermal variations are under way and will be published later.

Besides the measurements of complete sets of *hkl* presented above, the thermal variation of the six first reflections (010, 011, 020, 021, 030 and 002), which was measured to follow the polarization temperature dependence, is also very fruitful. This diffuse contribution is observable only at low $\sin\theta/\lambda$. The experimental values for the reflection 010 ($\sin\theta/\lambda = 0.106$ Å^{-1}) and for the reflection 021 ($\sin\theta/\lambda = 0.268$ Å^{-1}) are compared in figure 5. They are the sums of the diffuse and 4f localized contributions, and because of the negative character of the polarization, the values measured for the 010 reflection at low temperature are in fact below those measured for the 021. The corresponding magnetic amplitudes for the 4f cerium moment have been calculated with the set of parameters given above and they are also shown in figure 5. Whereas there is almost no difference between observed and calculated points for the 021 reflection, a large difference is observed for the 010 reflection. This difference disappears on warming up to around 115 K, confirming that the polarization vanishes at the ordering temperature.

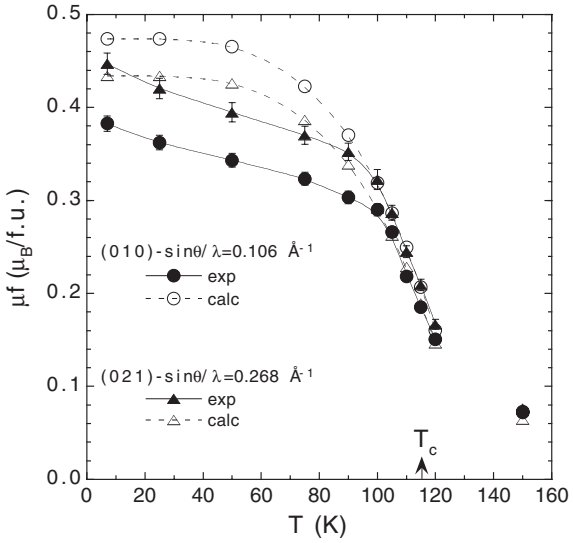

Figure 5. Thermal variation of the magnetic amplitudes μf of the 010 (circles) and 021 (triangles) reflections. Full dots are experimental results, open dots are calculated points and lines are guides for the eye. The data at $T = 150$ K were obtained in a different magnetic field, $H = 9$ T instead of 5 T.

5. Discussion

5.1. Diffuse polarization

Both analyses of the polarized neutron results, in direct or reciprocal space, show that the strong and negative diffuse magnetic density is present essentially in the ferromagnetic state.

From the magnetization density maps which provide the localization of the projected density, we find that this diffuse negative density is anisotropic and located mostly along the $\boldsymbol{c}$-chains. The map at $T = 150$ K, in the paramagnetic state, shows that it has strongly decreased. The mean value of the negative densities between two cerium atoms gives an approximate idea of the amplitude of the polarization. It is reported in figure 6(a) for the two directions [001] and [210] (full and open squares, respectively).

From the form factor analysis, we get values of the calculated cerium localized 4f moments μ_{4f} either from refinements at 7, 110, 120 and 150 K (table 3) or by calculation at various temperatures between 7 and 150 K with the set of parameters given above ($(B_2^0)_c = -7500$ K, $(B_4^0)_c = 650$ K, $(B_6^0)_c = -350$ K, $(B_6^6)_c = 0$, $J_{ff} = 570$ K and $K_0 = 0.67$). They are reported in figure 6(a) and, by comparison with the macroscopic magnetization M, a mean value of the macroscopic negative polarization ($M - \mu_{4f}$) can be deduced. The values thus obtained at different temperatures (crosses) are slightly lower than those along the [001] axis deduced from the maps (full squares). In fact, they do not match exactly to the same polarization: the former correspond to a macroscopic polarization in the cell, whereas the latter represent the mean polarization along one direction. But they are very close and present similar variations, confirming that the negative polarization of the cell is mostly located along the [001] direction.

The diffuse negative magnetization ($M - \mu_{4f}$) disappears at the ordering temperature. In fact, as can be seen in figure 6(b), this polarization presents a linear variation versus the calculated spin part μ_{4f}^S of the 4f moment μ_{4f}, and even becomes positive for very small values of μ_{4f}^S. Because of the uncertainty on measurements of such small moments and on the

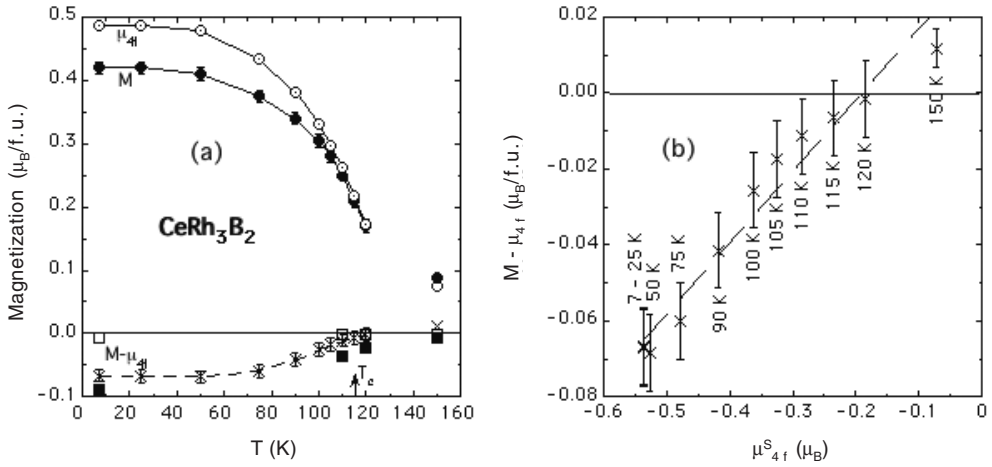

Figure 6. (a) Thermal variation of the measured macroscopic magnetization M (full circles), of the calculated 4f moment μ_{4f} (open circles) and of the diffuse negative polarization (crosses). Lines are guides for the eye. Squares are the mean values deduced from the maps between two cerium atoms in the directions [001] (full dots) and [210] (open dots). The data at $T = 150$ K were obtained in a different magnetic field, $H = 9$ T instead of 5 T. (b) Diffuse negative polarization versus the spin part of the 4f moment.

parameters used for the calculations, this result has to be treated with great caution. However, a similar result had already been observed in the 3d nickel metal by Brown *et al* [12].

5.2. Two-multiplet calculations

The influence of the excited multiplet of the Ce^{3+} ion is found to be far from negligible. At $T = 7$ K, the 4f moment μ_{4f} is smaller when calculated with two multiplets than with one multiplet (see table 2). The difference from the experimental macroscopic magnetization $M = 0.42\ \mu_B$, which determines the amplitude of the diffuse polarization, is then lowered by a factor of 2.

In contrast, the calculated spin contribution μ^S_{4f} to the 4f moment is higher with two multiplets than with one multiplet (see tables 2 and 3). As the exchange interaction

$$\mathcal{H}_{Ex} = -2J_{ff}\langle S\rangle \boldsymbol{S}$$

is related to the value of the spin, the same value of the exchange parameter J_{ff} will lead to exchange effects that are much more important when the second multiplet is involved. The important crystal field in $CeRh_3B_2$, which implies an influence of the second multiplet, might be a part of the explanation for the abnormally high ordering temperature of that compound.

Such enhancement of the spin contribution is in agreement with results of magnetic Compton effect measurements [13, 14] that give the value of the spin moment of the whole compound. Analysis of the Compton profiles leads in both studies to the conclusion that the ratio of the orbital to the spin part of the 4f moment $-\mu^L_{4f}/\mu^S_{4f}$ is abnormally low (between 2.9 [13] and 1.8 [14]), compared to the value of 4 expected from Hund's rules applied to the fundamental multiplet of the Ce^{3+} ion. From our calculations with two multiplets, we find that $\mu^S_{4f} \simeq -\mu_{4f}$ at all temperatures (see table 3), leading to $\mu^L_{4f} \simeq -2\mu^S_{4f}$. The low value of the ratio $-\mu^L_{4f}/\mu^S_{4f}$ then originates from the value of the spin part which is higher than usually expected for a same value of the total moment μ_{4f}.

6. Conclusion

This study demonstrates the essential role played by the huge crystal electric field in $CeRh_3B_2$ in its magnetic properties. Because of the large splitting, the influence of the second multiplet of the Ce^{3+} ion state is not negligible. In particular, it leads to a lower value of the 4f moment, associated with an enhancement of its spin part. This latter point could explain the abnormally high Curie temperature of this compound.

Such high crystal field effects are related to the crystal structure of $CeRh_3B_2$, with very short distances between cerium atoms along the c-direction, much shorter than in the c-plane. This feature leads to very anisotropic properties and to strong hybridization between cerium 4f and conduction electrons along that direction. A diffuse negative magnetic density is indeed present along the c-chains in the ordered state and disappears on heating above the Curie temperature.

Acknowledgments

The authors would like to acknowledge J Schweizer for many fruitful discussions. They also thank G Fillion for the magnetization measurements, which were performed at the Néel Laboratory, CNRS, Grenoble, France.

Appendix A. Calculation of the magnetic form factor for rare earth ions taking into account several multiplets J

A.1. Formalism

The magnetic form factor of a 4f ion for neutron diffraction is obtained from the cross section of the neutron due to the interaction of its spin with the magnetic field existing in the target. This field is mainly due to the spin of the electrons and to the motion of their charges (spin and orbital parts, respectively). This interaction can be evaluated from the matrix elements of the operator $\hat{\boldsymbol{Q}}_\perp(\boldsymbol{\kappa})$ between the initial and final states $|\mu\rangle$ and $|\mu'\rangle$ of the target, using the tensor operator method [15, 16]:

$$\langle\mu|\hat{\boldsymbol{Q}}_\perp(\boldsymbol{\kappa})|\mu'\rangle$$

with

$$\hat{\boldsymbol{Q}}_\perp(\boldsymbol{\kappa}) = \tilde{\boldsymbol{\kappa}} \times \hat{\boldsymbol{Q}}(\boldsymbol{\kappa}) \times \tilde{\boldsymbol{\kappa}}$$

where $\hat{\boldsymbol{Q}}(\boldsymbol{\kappa})$ is an intermediate operator related to the magnetization density in direct space and $\boldsymbol{\kappa}$ the scattering vector:

$$\tilde{\boldsymbol{\kappa}} = \frac{\boldsymbol{\kappa}}{|\boldsymbol{\kappa}|}.$$

With the assumption that the states of the neutrons can be described by plane waves $\exp(\mathrm{i}\boldsymbol{\kappa}\cdot\boldsymbol{r})$:

$$\hat{\boldsymbol{Q}}(\boldsymbol{\kappa}) = \exp(\mathrm{i}\boldsymbol{\kappa}\cdot\boldsymbol{r})\left(\hat{\boldsymbol{s}} - \frac{\mathrm{i}}{\hbar|\boldsymbol{\kappa}|}\tilde{\boldsymbol{\kappa}} \times \hat{\boldsymbol{p}}\right)$$

where $\hat{\boldsymbol{s}}$ and $\hat{\boldsymbol{p}}$ are the spin and momentum operators for the electron.

The radial part of the 4f wavefunction $f(r)$ is only present in the radial integrals $\langle j_K(\kappa)\rangle$, where $j_K(\kappa r)$ is a Bessel function:

$$\langle j_K(\kappa)\rangle = \int_0^\infty r^2\,\mathrm{d}r\,|f(r)|^2 j_K(\kappa r).$$

They can be found in [17], as a result of a relativistic Dirac–Fock method which is well adapted for the rare earth ions.

The n electrons of the configuration l^n ($l = 3$ for rare earths) couple to give total S, L and J. The summation over the n electrons and the transformation from one electron wavefunction $|lm\rangle$ to $|\theta JM\rangle$ is performed by Racah algebra [18], using parent states defined by $\bar{S}$, $\bar{L}$ and coefficients of fractional parentage (cfp) [19] (see table A.1). $\theta = \nu SL$, where the symbol ν stands for any other quantum numbers that are needed when the set $SM_S LM_L$ fails to define the state uniquely. The wavefunction is then

$$|\psi\rangle = \sum_{JM} a_{JM}|\theta JM\rangle.$$

The components $\hat{\boldsymbol{Q}}_\perp(\boldsymbol{\kappa})_q$ are calculated from

$$\begin{aligned}\langle\theta JM|\hat{\boldsymbol{Q}}_\perp(\boldsymbol{\kappa})_q|\theta' J'M'\rangle &= \Big\langle\theta JM\Big|\sum_{\text{electrons}} \exp(\mathrm{i}\boldsymbol{\kappa}\cdot\boldsymbol{r})\Big[\tilde{\boldsymbol{\kappa}}\times(\hat{\boldsymbol{s}}\times\tilde{\boldsymbol{\kappa}}) - \frac{\mathrm{i}}{\hbar|\boldsymbol{\kappa}|}\tilde{\boldsymbol{\kappa}}\times\hat{\boldsymbol{p}}\Big]_q|\theta' J'M'\rangle \\ &= (4\pi)^{1/2}\sum_{KK'}\{A_{J,J'}(K,K') + B_{J,J'}(K,K')\} \\ &\quad\times\sum_{QQ'} Y_K^Q(\tilde{\boldsymbol{\kappa}})\langle K'Q'J'M'|JM\rangle\langle KQK'Q'|1q\rangle,\end{aligned}$$

where $A_{J,J'}(K,K')$ is the orbital contribution, $B_{J,J'}(K,K')$ is the spin contribution, containing both $3j$, $6j$, $9j$ symbols and the summation over the parent states. $\langle K'Q'J'M'|JM\rangle$ and $\langle KQK'Q'|1q\rangle$ are Clebsh–Gordan coefficients and $Y_K^Q(\tilde{\boldsymbol{\kappa}})$ a spherical harmonic. For rare earths it is possible to consider only the lowest SL term. Then $\theta' = \theta$ and $S' = S$, $L' = L$. The orbital contribution $A_{JJ'}(K,K')$ can be expressed as a function of coefficients $a_{JJ'}(K,K')$ [16, 20]:

$$A_{J,J'}(K,K') = a_{J,J'}(K,K')[\langle j_{K'-1}(\kappa)\rangle + \langle j_{K'+1}(\kappa)\rangle].$$

The spin contribution is more complicated, especially when several multiplets are involved. As for the orbital part it is possible to express $B_{J,J'}(K,K')$ as a function of coefficients $c_{JJ'}(K,K')$ [16, 20]:

- if K' is odd, then $K = K' \pm 1$:

$$\begin{aligned}B_{J,J'}(K'-1,K') = \frac{\mathrm{i}^{K'-1}}{\sqrt{3(2K'+1)}}\big[&(K'+1)c_{JJ'}(K'-1,K')\langle j_{K'-1}(\kappa)\rangle \\ &- \sqrt{K'(K'+1)}c_{JJ'}(K'+1,K')\langle j_{K'+1}(\kappa)\rangle\big];\end{aligned}$$

- if K' is even, then $K = K'$:

$$B_{J,J'}(K',K') = \mathrm{i}^{K'}\sqrt{\frac{(2K'+1)}{3}}c_{JJ'}(K',K')\langle j_{K'}(\kappa)\rangle.$$

If only the ground multiplet is involved ($J' = J$), $B_{J,J}(K',K')$ is zero if $K = K'$, due to the $9j$ coefficient present in $c_{JJ'}(K,K')$.

A.2. Calculations of $a_{JJ'}$ and $c_{JJ'}$ coefficients

The coefficients $A_{JJ'}(K,K')$ and $B_{JJ'}(K,K')$ are tabulated for $J' = J$ in [20], and for $J' = J$ and $J' = J+1$ (for light rare earths) or $J' = J-1$ (for heavy rare earths) in [16]. For our calculations, which include several multiplets, we need the other coefficients. From the complete formalism [15], we have written a program which can calculate the $a_{JJ'}(K,K')$

Table A.1. Quantum numbers for l^n, parent states ($\bar{S}$ and $\bar{L}$) for l^{n-1} and coefficients of fractional parentage (cfp) [19] for Ce^{3+} and Sm^{3+}.

Ion	Config.	S	L	J	Ground state	Parents	$\bar{S}$	$\bar{L}$	cfp
Ce^{3+}	$4f^1$	1/2	3	5/2	$^2F_{5/2}$	^1S	1/2	0	1
Sm^{3+}	$4f^5$	5/2	5	5/2	$^6H_{5/2}$	^5D	2	2	$-(2/(3\times 7))^{1/2}$
						^5F	2	3	$-(1/(2\times 5))^{1/2}$
						^5G	2	4	$-((3\times 13)/(2\times 7\times 11))^{1/2}$
						^5I	2	6	$+((7\times 13)/(3\times 5\times 11))^{1/2}$

Table A.2. Coefficients $A(K, K')$ and $B(K, K')$ as a function of $a(K, K')$ and $c(K, K')$ for f electrons.

K	K'	$A(K, K')$	$B(K, K')$
0	1	$a(0,1)[\langle j_0\rangle + \langle j_2\rangle]$	$\frac{2}{3}c(0,1)\langle j_0\rangle - \frac{\sqrt{2}}{3}c(2,1)\langle j_2\rangle$
2	1	$\sqrt{\frac{1}{2}}a(0,1)[\langle j_0\rangle + \langle j_2\rangle]$	$\sqrt{\frac{1}{2}}\left[\frac{2}{3}c(0,1)\langle j_0\rangle - \frac{\sqrt{2}}{3}c(2,1)\langle j_2\rangle\right]$
2	2		$-\sqrt{\frac{5}{3}}c(2,2)\langle j_2\rangle$
2	3	$a(2,3)[\langle j_2\rangle + \langle j_4\rangle]$	$-\frac{4}{\sqrt{21}}c(2,3)\langle j_2\rangle + \frac{2}{\sqrt{7}}c(4,3)\langle j_4\rangle$
4	3	$\sqrt{\frac{3}{4}}a(2,3)[\langle j_2\rangle + \langle j_4\rangle]$	$\sqrt{\frac{3}{4}}\left[-\frac{4}{\sqrt{21}}c(2,3)\langle j_2\rangle + \frac{2}{\sqrt{7}}c(4,3)\langle j_4\rangle\right]$
4	4		$\sqrt{3}c(4,4)\langle j_4\rangle$
4	5	$a(4,5)[\langle j_4\rangle + \langle j_6\rangle]$	$\frac{6}{\sqrt{33}}c(4,5)\langle j_4\rangle - \sqrt{\frac{10}{11}}c(6,5)\langle j_6\rangle$
6	5	$\sqrt{\frac{5}{6}}a(4,5)[\langle j_4\rangle + \langle j_6\rangle]$	$\sqrt{\frac{5}{6}}\left[\frac{6}{\sqrt{33}}c(4,5)\langle j_4\rangle - \sqrt{\frac{10}{11}}c(6,5)\langle j_6\rangle\right]$
6	6		$-\sqrt{\frac{13}{3}}c(6,6)\langle j_6\rangle$
6	7	—	$-\frac{8}{\sqrt{45}}c(6,7)\langle j_6\rangle$
8	7	—	$\sqrt{\frac{7}{8}}\left[-\frac{8}{\sqrt{45}}c(6,7)\langle j_6\rangle\right]$

and $c_{JJ'}(K, K')$ coefficients for the different rare earth ions, including the cfp and $3j$, $6j$ and $9j$ coefficients.

The calculation with several multiplets is always necessary for the Sm^{3+} ion, whereas for the Ce^{3+} ion this calculation has to be done only in some special physical cases. These two ions present the same ground multiplet $J = 5/2$ and this rather low value implies that, due to the $9j$ coefficient present in $c_{JJ'}(K, K')$, these coefficients are non-zero only if $K' \leqslant J' + J$. The terms $c_{JJ'}(6, 7)$ and then $B_{JJ'}(6, 7)$ and $B_{JJ'}(8, 7)$ are different from zero only for $J + J' \geqslant 7$. But these two ions differ in their number of 4f electrons. In the case of Ce^{3+}, only one 4f electron is present and there is then only one parent. For Sm^{3+}, with five 4f electrons, four parents must be taken into account (see table A.1). S and L not being the same for the two ions, there are only two multiplets $J = 3 \pm 1/2$ in Ce^{3+}, and there are six multiplets between $J = 5 - 5/2$ and $5 + 5/2$ in Sm^{3+}. We present coefficients calculated for both ions Ce^{3+} and Sm^{3+} in tables A.2–A.5.

A.3. Form factor calculations using the wavefunction

We have written a program calculating the magnetic form factor of the ground state from the wavefunction. It is a generalization of that previously developed [21] and it uses the

Table A.3. Coefficients $a_{J,J'}(K, K')$ and $c_{J,J'}(K, K')$ for Ce^{3+} and Sm^{3+} ions for the two multiplets 5/2 and 7/2. The coefficients in bold can also be obtained from those tabulated by Balcar and Lovesey [16] and/or Lander and Brun [20].

				Ce^{3+} ion		Sm^{3+} ion	
J	J'	K	K'	$a_{J,J'}(K, K')$	$c_{J,J'}(K, K')$	$a_{J,J'}(K, K')$	$c_{J,J'}(K, K')$
5/2	5/2	0	1	**−1.126 87**	**0.422 58**	**−1.690 31**	**2.112 89**
5/2	5/2	2	1	**−0.796 82**	**0.478 09**	**−1.195 23**	**−0.345 29**
5/2	5/2	2	2	—	**0**	—	**0**
5/2	5/2	2	3	**−0.521 64**	**−0.239 05**	**0**	**0.172 64**
5/2	5/2	4	3	**−0.451 75**	**−0.690 07**	**0**	**−0.271 84**
5/2	5/2	4	4	—	**0**	—	**0**
5/2	5/2	4	5	**−0.217 31**	**0.104 03**	**0.085 61**	**0.040 98**
5/2	5/2	6	5	**−0.198 38**	**1.139 61**	**0.078 15**	**0.195 69**
5/2	5/2	6	6	—	**0**	—	**0**
5/2	5/2	6	7	—	**0**	—	**0**
5/2	7/2	0	1	**0.251 98**	**−0.755 93**	**0.690 07**	**−2.070 20**
5/2	7/2	2	1	**0.178 17**	**0.267 26**	**0.487 95**	**0.042 29**
5/2	7/2	2	2	—	**0.623 61**	—	**−0.164 46**
5/2	7/2	2	3	**0.329 91**	**0.503 95**	**0**	**−0.292 38**
5/2	7/2	4	3	**0.285 71**	**−0.327 33**	**0**	**0.204 03**
5/2	7/2	4	4	—	**−0.690 85**	—	**−0.099 38**
5/2	7/2	4	5	**0.343 60**	**−0.394 77**	**−0.247 13**	**−0.151 43**
5/2	7/2	6	5	**0.313 67**	**0.300 31**	**−0.225 60**	**−0.433 10**
5/2	7/2	6	6	—	**0.940 13**	—	**0.058 95**
5/2	7/2	6	7	—	**0**	—	**0**
7/2	5/2	0	1	−0.218 22	0.654 65	−0.597 61	1.792 84
7/2	5/2	2	1	−0.154 30	−0.231 46	−0.422 58	−0.036 62
7/2	5/2	2	2	—	0.540 06	—	−0.142 42
7/2	5/2	2	3	−0.285 71	−0.436 44	0	0.253 21
7/2	5/2	4	3	−0.247 44	0.283 47	0	−0.176 70
7/2	5/2	4	4	—	−0.598 29	—	−0.086 06
7/2	5/2	4	5	−0.297 57	0.341 88	0.214 02	0.131 14
7/2	5/2	6	5	−0.271 64	−0.260 08	0.195 37	0.375 07
7/2	5/2	6	6	—	0.814 17	—	0.051 05
7/2	5/2	6	7	—	0	—	0
7/2	7/2	0	1	−1.133 89	−0.566 95	−1.553 85	0.692 93
7/2	7/2	2	1	−0.801 78	−0.267 26	−1.098 74	−0.293 39
7/2	7/2	2	2	—	0	—	0
7/2	7/2	2	3	−0.547 10	0.626 78	0	−0.141 56
7/2	7/2	4	3	−0.473 80	0.197 39	0	−0.200 44
7/2	7/2	4	4	—	0	—	0
7/2	7/2	4	5	−0.277 02	−0.795 69	−0.184 68	−0.227 19
7/2	7/2	6	5	−0.252 89	−0.111 75	−0.168 59	−0.099 78
7/2	7/2	6	6	—	0	—	0
7/2	7/2	6	7	—	1.236 82	—	0.220 88

$a_{JJ'}(K, K')$ and $c_{JJ'}(K, K')$ coefficients. The coefficients of the ground state wavefunction can be refined by a least squares method from the measured form factor. However, this method can be applied if only one level is populated: at high temperatures, where the population of several levels is important, a formalism involving the diagonalization of the Hamiltonian has then to be developed.

Table A.4. Coefficients $a_{J,J'}(K, K')$ and $c_{J,J'}(K, K')$ for a Sm^{3+} ion for the third multiplet $J = 9/2$.

J	J'	K	K'	$a_{J,J'}(K, K')$	$c_{J,J'}(K, K')$
5/2	9/2	0	1	0	0
5/2	9/2	2	1	0	0
5/2	9/2	2	2	—	0.123 36
5/2	9/2	2	3	0	0.227 88
5/2	9/2	4	3	0	−0.034 72
5/2	9/2	4	4	—	0.186 35
5/2	9/2	4	5	0.297 55	0.233 61
5/2	9/2	6	5	0.271 63	0.317 41
5/2	9/2	6	6	—	−0.264 24
5/2	9/2	6	7	—	−0.198 22
7/2	9/2	0	1	0.749 49	−2.248 46
7/2	9/2	2	1	0.529 97	−0.010 60
7/2	9/2	2	2	—	−0.218 78
7/2	9/2	2	3	0	−0.157 16
7/2	9/2	4	3	0	0.156 46
7/2	9/2	4	4	—	−0.099 68
7/2	9/2	4	5	−0.115 24	0.094 15
7/2	9/2	6	5	−0.105 20	−0.342 46
7/2	9/2	6	6	—	−0.024 42
7/2	9/2	6	7	—	−0.391 38
9/2	5/2	0	1	0	0
9/2	5/2	2	1	0	0
9/2	5/2	2	2	—	−0.095 55
9/2	5/2	2	3	0	0.176 52
9/2	5/2	4	3	0	−0.026 90
9/2	5/2	4	4	—	−0.144 35
9/2	5/2	4	5	0.230 48	0.180 95
9/2	5/2	6	5	0.210 40	0.245 87
9/2	5/2	6	6	—	0.204 68
9/2	5/2	6	7	—	−0.153 54
9/2	7/2	0	1	−0.670 36	2.011 08
9/2	7/2	2	1	−0.474 02	0.009 48
9/2	7/2	2	2	—	−0.195 68
9/2	7/2	2	3	0	0.140 57
9/2	7/2	4	3	0	−0.139 94
9/2	7/2	4	4	—	−0.089 16
9/2	7/2	4	5	0.103 08	−0.084 21
9/2	7/2	6	5	0.094 10	0.306 30
9/2	7/2	6	6	—	−0.021 85
9/2	7/2	6	7	—	0.350 06
9/2	9/2	0	1	−1.541 06	−0.351 76
9/2	9/2	2	1	−1.089 69	−0.225 52
9/2	9/2	2	2	—	0
9/2	9/2	2	3	0	−0.241 28
9/2	9/2	4	3	0	−0.212 76
9/2	9/2	4	4	—	0
9/2	9/2	4	5	−0.178 79	−0.186 76
9/2	9/2	6	5	−0.163 22	0.015 46
9/2	9/2	6	6	—	0
9/2	9/2	6	7	—	−0.088 21

Table A.5. Orbital contributions $A_{JJ'}(K, K')$ and spin contributions $B_{JJ'}(K, K')$ for the Ce^{3+} ion. The coefficients for 5/2, 5/2 and 5/2, 7/2 were tabulated by Balcar and Lovesey [16].

J	J'	K	K'	$A(K,K')$ $\langle j_0\rangle$	$B(K,K')$ $\langle j_0\rangle$	$A(K,K')$ $\langle j_2\rangle$	$B(K,K')$ $\langle j_2\rangle$	$A(K,K')$ $\langle j_4\rangle$	$B(K,K')$ $\langle j_4\rangle$	$A(K,K')$ $\langle j_6\rangle$	$B(K,K')$ $\langle j_6\rangle$
5/2	5/2	0	1	−1.126 87	0.281 72	−1.126 87	−0.225 37				
5/2	5/2	2	1	−0.796 82	0.199 20	−0.796 82	−0.159 36				
5/2	5/2	2	2			—	0				
5/2	5/2	2	3			−0.521 64	0.208 66	−0.521 64	−0.521 64		
5/2	5/2	4	3			−0.451 75	0.180 70	−0.451 75	−0.451 75		
5/2	5/2	4	4					—	0		
5/2	5/2	4	5					−0.217 31	0.108 66	−0.217 31	−1.086 57
5/2	5/2	6	5					−0.198 38	0.099 19	−0.198 38	−0.991 90
5/2	5/2	6	6							—	0
5/2	7/2	0	1	0.251 98	−0.503 95	0.251 98	−0.125 99				
5/2	7/2	2	1	0.178 17	−0.356 35	0.178 17	−0.089 09				
5/2	7/2	2	2			—	−0.805 08				
5/2	7/2	2	3			0.329 91	−0.439 89	0.329 91	−0.247 44		
5/2	7/2	4	3			0.285 71	−0.380 95	0.285 71	−0.214 29		
5/2	7/2	4	4					—	−1.196 59		
5/2	7/2	4	5					0.343 60	−0.412 32	0.343 60	−0.286 34
5/2	7/2	6	5					0.313 67	−0.376 40	0.313 67	−0.261 39
5/2	7/2	6	6							—	−1.957 03
7/2	5/2	0	1	−0.218 22	0.436 44	−0.218 22	0.109 11				
7/2	5/2	2	1	−0.154 30	0.308 61	−0.154 30	0.077 15				
7/2	5/2	2	2			—	−0.697 22				
7/2	5/2	2	3			−0.285 71	0.380 95	−0.285 71	0.214 29		
7/2	5/2	4	3			−0.247 44	0.329 91	−0.247 44	0.185 58		
7/2	5/2	4	4					0	−1.036 27		
7/2	5/2	4	5					−0.297 57	0.357 08	−0.297 57	0.247 97
7/2	5/2	6	5					−0.271 64	0.325 97	−0.271 64	0.226 37
7/2	5/2	6	6							—	−1.694 84
7/2	7/2	0	1	−1.133 89	−0.377 96	−1.133 89	0.125 99				
7/2	7/2	2	1	−0.801 78	−0.267 26	−0.801 78	0.089 09				
7/2	7/2	2	2			—	0				
7/2	7/2	2	3			−0.547 10	−0.547 10	−0.547 10	0.149 21		
7/2	7/2	4	3			−0.473 80	−0.473 80	−0.473 80	0.129 22		
7/2	7/2	4	4					0	0		
7/2	7/2	4	5					−0.277 02	−0.831 07	−0.277 02	0.106 55
7/2	7/2	6	5					−0.252 89	−0.758 66	−0.252 89	0.097 26
7/2	7/2	6	6							—	0
7/2	7/2	6	7								−1.474 99
7/2	7/2	8	7								−1.379 73

A.4. Form factor calculations using the Hamiltonian

We have also written a double-precision program calculating the magnetic form factor at any temperature using the complete Hamiltonian of appendix B. Starting from the spin–orbit coupling, from the crystal field parameters, from the exchange and applied fields, the energy levels and the wavefunctions are obtained by diagonalization. The magnetic form factor is then calculated for each level using the coefficients $a_{JJ'}(K, K')$ and $c_{JJ'}(K, K')$ previously obtained, and finally a thermal averaging is performed. A comparison between calculated and observed form factors leads to a refinement, by a least squares method, of the parameters of

the Hamiltonian. The calculations have been tested by a comparison to the results of ones performed in 1978 with the SCAMAG program [22] for Sm compounds [23].

Appendix B. Matrix elements of the Hamiltonian for rare earth ions in the case of J mixing

B.1. Formalism

To calculate physical variables, such as the moment and form factor, it is necessary to obtain the wavefunctions and the energies of the different levels by diagonalizing the total Hamiltonian, which can be written as the summation of four terms:

$$\mathcal{H} = \mathcal{H}_{\mathrm{SO}} + \mathcal{H}_{\mathrm{CF}} + \mathcal{H}_{\mathrm{Ex}} + \mathcal{H}_{\mathrm{Ap}}$$

with

$\mathcal{H}_{\mathrm{SO}}$: spin–orbit coupling term,

$\mathcal{H}_{\mathrm{CF}}$: crystal field term,

$\mathcal{H}_{\mathrm{Ex}}$: exchange term,

$\mathcal{H}_{\mathrm{Ap}}$: Zeeman term (applied field).

B.2. The spin–orbit coupling Hamiltonian

$$\mathcal{H}_{\mathrm{SO}} = \lambda \boldsymbol{L} \cdot \boldsymbol{S}.$$

The corresponding matrix is rather simple, diagonal (non-zero only if $J = J'$ and $M = M'$) and independent of M. The coefficient λ is related to the splitting between the multiplets:

$$\langle \theta J M | \lambda \boldsymbol{L} \cdot \boldsymbol{S} | \theta J' M' \rangle = (1/2)\lambda[J(J+1) - L(L+1) - S(S+1)].$$

B.3. The crystal field Hamiltonian

In order to include several multiplets, the method of the Stevens operators [24] set up for the calculation of matrix elements within the ground J multiplet is no longer convenient, and a more general approach has been developed. The crystal field potential V at a rare earth ion site can be expressed as [25]

$$V = \sum_{k,q} V_k^q = \sum_{k,q} A_k^q \langle r^k \rangle Y_k^q(\theta, \phi)$$

where $Y_k^q(\theta, \phi)$ is a spherical harmonic, $\langle r^k \rangle$ is the mean value of the kth power of the 4f electron radius, A_k^q are parameters related to the strength of the crystal field. It is possible to define

$$U_k^q = (4\pi/(2k+1))^{1/2} Y_k^q.$$

It as been shown [26] that the crystal field matrix elements of a configuration f^n can be calculated by the tensor operator techniques of Racah [18] (for one SL term) in terms of $3j$ and $6j$ symbols:

$$\langle \theta J M | U_k^q | \theta J' M' \rangle = \delta(SS')(-1)^{M+S+L}[(2J+1)(2J'+1)]^{1/2} \times \begin{pmatrix} J & k & J' \\ -M & q & M' \end{pmatrix} \begin{Bmatrix} L & J & S \\ J' & L & k \end{Bmatrix} \langle \nu SL \| U_k \| \nu SL \rangle.$$

If we use the normalization factors N_k^q, the A_k^q coefficients are similar to those involved in the Stevens formalism [24], and

$$\mathcal{H}_{\mathrm{CF}} = \sum_{k,q} N_k^q A_k^q \langle r^k \rangle U_k^q = \sum_{k,q} N_k^q B_k^q U_k^q.$$

The N_k^q coefficients and the reduced matrix elements $\langle \nu SL \| U_k \| \nu SL \rangle$ are tabulated in [25] but some errors seem to be present in that reference (appendix B.6).

B.4. The exchange Hamiltonian

The third term describes the effect of the exchange via the interionic exchange parameter J_{ff} acting on the spin operator $\boldsymbol{S}$:

$$\mathcal{H}_{\mathrm{Ex}} = -2J_{\mathrm{ff}}\langle S\rangle \boldsymbol{S}.$$

The reference [27] gives the matrix elements for S_z and S_x:

$$\langle \theta J M|S_z|\theta J' M'\rangle = (-1)^{J-M+L+S+J'+1}[(2J+1)(2J'+1)]^{1/2} \times \begin{pmatrix} J & 1 & J' \\ -M & 0 & M' \end{pmatrix} \begin{Bmatrix} S & S & 1 \\ J & J' & L \end{Bmatrix} [S(S+1)(2S+1)]^{1/2},$$

$$\langle \theta J M|S_x|\theta J' M'\rangle = (-1)^{J-M+L+S+J'+1}[(2J+1)(2J'+1)]^{1/2} \times \frac{1}{\sqrt{2}}\left[\begin{pmatrix} J & 1 & J' \\ -M & -1 & M' \end{pmatrix} - \begin{pmatrix} J & 1 & J' \\ -M & +1 & M' \end{pmatrix} \right] \begin{Bmatrix} S & S & 1 \\ J & J' & L \end{Bmatrix} \times [S(S+1)(2S+1)]^{1/2}.$$

With the relations

$$S_+ = S_x + \mathrm{i}S_y, \qquad S_x = (1/2)(S_- + S_+),$$
$$S_- = S_x - \mathrm{i}S_y, \qquad S_y = (\mathrm{i}/2)(S_- - S_+),$$

it is then easy to obtain the matrix elements of S_y, S_+, and S_-:

$$\langle \theta J M|S_y|\theta J' M'\rangle = \mathrm{i}(-1)^{J-M+L+S+J'+1}[(2J+1)(2J'+1)]^{1/2} \times \frac{1}{\sqrt{2}}\left[\begin{pmatrix} J & 1 & J' \\ -M & -1 & M' \end{pmatrix} + \begin{pmatrix} J & 1 & J' \\ -M & +1 & M' \end{pmatrix} \right] \begin{Bmatrix} S & S & 1 \\ J & J' & L \end{Bmatrix} \times [S(S+1)(2S+1)]^{1/2},$$

$$\langle \theta J M|S_+|\theta J' M'\rangle = -\sqrt{2}(-1)^{J-M+L+S+J'+1}[(2J+1)(2J'+1)]^{1/2} \times \begin{pmatrix} J & 1 & J' \\ -M & +1 & M' \end{pmatrix} \begin{Bmatrix} S & S & 1 \\ J & J' & L \end{Bmatrix} [S(S+1)(2S+1)]^{1/2},$$

$$\langle \theta J M|S_-|\theta J' M'\rangle = \sqrt{2}(-1)^{J-M+L+S+J'+1}[(2J+1)(2J'+1)]^{1/2} \times \begin{pmatrix} J & 1 & J' \\ -M & -1 & M' \end{pmatrix} \begin{Bmatrix} S & S & 1 \\ J & J' & L \end{Bmatrix} [S(S+1)(2S+1)]^{1/2}.$$

B.5. The Zeeman Hamiltonian

The fourth term describes the effect of the applied field $\boldsymbol{H}_{\mathrm{Ap}}$ acting on the moment operator:

$$\mathcal{H}_{\mathrm{Ap}} = \mu_{\mathrm{B}}\boldsymbol{H}_{\mathrm{Ap}} \cdot (\boldsymbol{L} + 2\boldsymbol{S}).$$

The reference [27] gives the matrix elements for L_z:

$$\langle \theta J M|L_z|\theta J' M'\rangle = (-1)^{J-M+L+S+J+1}[(2J+1)(2J'+1)]^{1/2} \times \begin{pmatrix} J & 1 & J' \\ -M & 0 & M' \end{pmatrix} \begin{Bmatrix} L & L & 1 \\ J & J' & S \end{Bmatrix} [L(L+1)(2L+1)]^{1/2}.$$

Table B.1. Modified sixth-order reduced matrix elements of the lowest SL term.

Ion	Ground term	$\langle \nu SL \| U_6 \| \nu SL \rangle$
Pr^{3+} Tm^{3+}	^3H	$\mp(1/3)(5 \times 17/7)^{1/2}$
Sm^{3+} Dy^{3+}	^6H	$\pm(1/3)(5 \times 17/7)^{1/2}$

As in the case of the spin, it is easy to obtain the expressions for L_+, L_-, L_x and L_y, and then those for J_z, J_x and J_y.

B.6. Diagonalization of the total Hamiltonian

A double-precision program diagonalizes the complex matrix of the total Hamiltonian. The field can be applied in any direction, and the self-consistency of the moments is achieved for any component. Some physical observables, such as magnetization, hyperfine field and neutron transitions can be calculated.

On comparing the formalisms of [25] and [27], a disagreement appears concerning the sign of the coefficients $\langle \nu SL \| U_6 \| \nu SL \rangle$ for Pr^{3+}, Sm^{3+}, Dy^{3+} and Tm^{3+}. Testing the calculations for a single multiplet J with a previous program, and comparing with calculations performed on Sm compounds [23], we agree with the formalism of [27]. The reduced elements are those of table B.1. Moreover, these tests demonstrate that the N_2^2 coefficient in [25] is half its real value and the exact value should be

$$N_2^2 = -4(7/3 \times 5)^{1/2} \times (2 \times 3)^{1/2}.$$

References

[1] Dhar S K, Malik S K and Vijayaraghavan R 1981 *J. Phys. C: Solid State Phys.* **14** L321
[2] Kasaya M, Okabe A, Takahashi T, Satoh T, Kasuya T and Fujimori A 1988 *J. Magn. Magn. Mater.* **76/77** 347
[3] Galatanu A, Yamamoto E, Okubo T, Yamada M, Thamizhavel A, Takeuchi T, Sugiyama K, Inada Y and Ōnuki Y 2003 *J. Phys.: Condens. Matter* **15** S2187
[4] Malik S K, Umarji A M, Shenoy G K, Montano P A and Reeves M E 1985 *Phys. Rev.* B **31** 4728
[5] Yamaguchi K, Namatame H, Fujimori A, Koide T, Shidara T, Nakamura M, Misu A, Fukutani H, Yuri M and Kasuya T 1995 *Phys. Rev.* B **51** 13952
[6] Givord F, Boucherle J-X and Murani A P 2000 *ISIS Experimental Report* No 11083
Givord F, Boucherle J-X, Murani A P and Bewley P 2004 at press
[7] Osborn R, Lovesey S W, Taylor A D and Balcar E 1991 *Handbook on the Physics and Chemistry of Rare Earth* vol 14 (Amsterdam: Elsevier)
[8] Alonso J A, Boucherle J-X, Givord F, Schweizer J, Gillon B and Lejay P 1998 *J. Magn. Magn. Mater.* **177–181** 1048
[9] Papoular R J and Gillon B 1990 *Europhys. Lett.* **13** 429
[10] Hutchings M T 1964 *Solid State Physics* vol 16 (New York: Academic) p 227
[11] Shaheen S A, Schilling J S and Shelton R N 1985 *Phys. Rev.* B **31** 656
[12] Brown P J, Déportes J and Ziebeck K R A 1991 *J. Physique* **1** 1529
[13] Yaouanc A, Dalmas de Réotier P and Sanchez J-P 1998 *Phys. Rev.* B **57** R681
[14] Sakurai Y, Itou M, Tamoura J, Nanao S, Thamizhavel A, Inada Y, Galatanu A, Yamamoto E and Ōnuki Y 2003 *J. Phys.: Condens. Matter* **15** S2183
[15] Lovesey S W 1984 *Theory of Neutron Scattering from Condensed Matter* (Oxford: Oxford University Press)
[16] Balcar E and Lovesey S W 1989 *Theory of Magnetic Neutron and Photon Scattering* (Oxford: Clarendon)
[17] Freeman A J and Desclaux J-P 1979 *J. Magn. Magn. Mater.* **12** 11
[18] Racah G 1943 *Phys. Rev.* **63** 367
[19] Nielson C W and Koester G F 1963 *Spectroscopic Coefficients for the p^n, d^n, and f^n Configurations* (Cambridge, MA: MIT Press)

[20] Lander G H and Brun T O 1970 *J. Chem. Phys.* **53** 1387
[21] Boucherle J-X 1977 *Thesis* University of Grenoble
[22] Balcar E, Lovesey S W and Rimmer R E 1975 *SCAMAG Program(ILL)*
[23] Boucherle J-X, Givord D, Laforest J, Schweizer J and Tasset F 1979 *J. Physique Coll.* **40** C5 180
[24] Stevens K W H 1952 *Proc. R. Soc.* A **65** 209
[25] Weber M J and Bierig R W 1964 *Phys. Rev.* A **134** 1492
[26] Elliott J P, Judd B R and Runciman W A 1957 *Proc. R. Soc.* A **240** 509
[27] De Wijn H W, Van Diepen A M and Buschow K H J 1976 *Phys. Status Solidi* b **76** 11